Mechanisms of Single-Walled Carbon Nanotube Probe−Sample Multistability in Tapping Mode AFM Imaging

Santiago D. Solares,[‡,§] Maria J. Esplandiu,[†,||] William A. Goddard, III,*[,†,§] and C. Patrick Collier*[,†]

Division of Chemistry and Chemical Engineering, California Institute of Technology, Pasadena, California 91125

Received: March 15, 2005; In Final Form: April 24, 2005

When using single-walled carbon nanotube (SWNT) probes to create AFM images of SWNT samples in tapping mode, elastic deformations of the probe and sample result in a decrease in the apparent width of the sample. Here we show that there are two major mechanisms for this effect, smooth gliding and snapping, and compare their dynamics to the case when a conventional silicon tip is used to image a bare silicon surface. Using atomistic and continuum simulations, we analyze in detail the shape of the tip−sample interaction potential for three model cases and show that in the absence of adhesion and friction forces, more than two discrete, physically meaningful solutions of the oscillation amplitude are possible when snapping occurs (in contrast to the existence of one attractive and one repulsive solution for conventional silicon AFM tips). We present experimental results indicating that a continuum of amplitude solutions is possible when using SWNT tips and explain this phenomenon with dynamic simulations that explicitly include tip−sample adhesion and friction forces. We also provide simulation results of SWNT tips imaging Si(111)−CH_3 surface step edges and Au nanocrystals, which indicate that SWNT probe multistability may be a general phenomenon, not limited to SWNT samples.

Introduction

Carbon nanotubes have been used successfully as AFM tips to image a variety of samples, including surfaces, biomolecules, and other types of nanoscale samples in both contact and noncontact mode.[1−7,9,10] These scanning probes have shown significant potential for numerous applications, due to their robustness, flexibility, small dimensions, and chemical stability, which can lead to reduced sample damage and finer resolution imaging than can be obtained with conventional silicon tips.[2,3,8−10] SWNTs are of particular interest due to their macromolecular-scale dimensions.

Theoretical and experimental studies of AFM tapping-mode imaging have shown that this process is subject to bistability, i.e., it is possible to obtain two solutions of the AFM cantilever oscillation amplitude for a given set of imaging parameters. It has also been shown that there are cases where more than two solutions are mathematically possible but for which only two of them are physically meaningful.[11] Since the AFM imaging process in tapping mode depends on the oscillation amplitude of the cantilever, good images require that the regions where bistability occurs be avoided. Often there is no systematic procedure to do this, and AFM operators have to rely on their intuition and previous experience.

It is known that the two solutions of the oscillation amplitude of the cantilever occur depending on whether the *average* gradient of the tip−sample interaction force is positive or negative.[11,12] In general, a typical tip−sample interaction potential contains a long-range attractive region and a short-range repulsive region, as do the well-known Morse and Lennard-Jones potentials, for example. The gradient of the tip−sample interaction force (negative of the second derivative of the potential with respect to the tip position) is positive in most of the attractive region, and is negative in most of the repulsive region. If the region of positive force gradient dominates the tip−sample interaction for a given set of imaging parameters (attractive regime), the resulting phase shift of the AFM tip oscillation relative to the excitation force will be greater than 90°, and if the region of negative force gradient dominates (repulsive regime) the phase shift will be below 90°.[11,12] Note that throughout this paper we use the terms "phase" and "phase shift" interchangeably.

This study uses a previously reported simulation methodology based on molecular dynamics (MD) and classical AFM dynamics (AFMD)[13] to show that the tip−sample interaction between SWNT AFM tips and samples does not always correspond to a simple potential like the one described above, and that the interaction between the tip and the sample can give rise to potentials of different shapes, which may give more than two physically meaningful solutions for the oscillation amplitude during tapping-mode AFM imaging. We also show that if tip−sample adhesion and friction forces are significant, it is possible to obtain a continuum of amplitude solutions, all of which are physically meaningful. In such cases it is more appropriate to speak of imaging multistability rather than bistability (we note that this type of effective multistability due to the combination of sample and substrate interaction potentials with nonconservative forces is different than the one described in refs 11 and 12, where a single interaction potential gives rise to two different oscillation states).

* Corresponding authors. E-mail: collier@caltech.edu, wag@wag.caltech.edu.
† Department of Chemistry.
‡ Department of Chemical Engineering.
§ Materials and Process Simulation Center.
|| Present address: Departament de Quimica, Universitat Autonoma de Barcelona.

10.1021/jp051363u CCC: $30.25
Published on Web 05/24/2005

TABLE 1: Geometry and AFM Simulation Parameters

Geometry Parameters	
silicon tip radius, imaging end	17 nm
silicon tip, base of pyramid	6800 nm
silicon tip length	17500 nm
SWNT tip diameter	5.5 nm (simulated as a 40,40 SWNT)
SWNT tip length	40 nm
SWNT tip tilt angle	15 degrees
sample SWNT diameter	2.1 nm (simulated as a 16,16 SWNT)
Imaging Parameters	
AFM cantilever force constant	4.8 N/m
AFM cantilever resonant frequency	47.48 kHz
AFM cantilever quality factor	150
integration time step	0.1 ns
integration time	0.02 s
calculated cantilever effective mass	5.3933×10^{-11} kg

Specifically, we analyze the tip−sample interaction potential of a SWNT AFM tip imaging a prone SWNT on a flat substrate. We have previously reported that for these systems it is possible to obtain a measured sample width that is smaller than the true sample width due to the elastic deformation of the tip and sample, which slide past one another.[13] Here we show that this sliding phenomenon can occur in two different modes, one where the tip and sample glide smoothly past one another, and a second mode in which the tip initially compresses the sample and then snaps off, involving a sudden lateral "jump" to the side of the sample. In the absence of tip−sample adhesion and friction forces, the first mode gives rise to two amplitude solutions (as is typical with conventional silicon tips), and the second mode gives rise to four solutions due to the existence of two regions where the gradient of the tip−sample interaction force is positive and two regions where it is negative. In the presence of tip−sample adhesion and friction forces, these sliding phenomena can give rise to a continuum of amplitude solutions, which exhibit smooth, continuous transitions between the attractive and repulsive regimes, in contrast to the discontinuities observed when using conventional silicon tips.

Finally we describe theoretical simulations of Si(111)−CH_3 surface step edges and Au nanocrystals, which show that SWNT probe multistability is a general phenomenon that can occur for a wide variety of samples, whenever snapping of the nanotube probe takes place.

Methods

Experimental. The fabrication, characterization and imaging process employed using SWNT tips has been previously described.[6] A Digital Instruments (Santa Barbara, CA) Multimode atomic force microscope with a Nanoscope IV controller was used for this work. As-grown SWNTs were mounted onto silicon AFM tips (FESP, NanoWorld) using the pick-up technique developed by Lieber and co-workers.[14] The experimental results presented here correspond to a SWNT AFM tip with diameter and length of approximately 5.5 and 40 nm respectively, tilted 15 degrees with respect to the vertical direction (a transmission electron microscopy image of this probe[6,13] is provided in the Supporting Information), mounted on a silicon tip with dimensions given in Table 1. These experimental results correspond to tapping-mode measurements for which the AFM tip was oscillating directly above the SWNT sample (a detailed procedure is provided in the Supporting Information). The relevant imaging and geometry parameters are listed in Table 1 and are the same as those used in the theoretical simulations. The cantilever driving frequency was the same as the resonance frequency in all cases.

Theoretical. The MD/AFMD simulation methodology has also been previously described.[13] It consists of modeling the AFM cantilever tip as a point mass using the damped harmonic oscillator equation of motion with the introduction of tip−sample interaction forces obtained through atomistic simulations of tip and sample. Our tip−sample interaction potentials include both short- and long-range van der Waals interactions between each atom in the tip (both the SWNT and the supporting silicon tip), and the sample and substrate. The long-range interactions are introduced as a correction to the molecular simulation result via the Hamaker equation for an atom (for each atom in the SWNT tip) or a sphere (for the Si tip) interacting with the surface of a semi-infinite solid (MD calculations usually neglect long-range attractive interactions since they use cutoffs on the order of 1 nm in the calculation of van der Waals interactions).

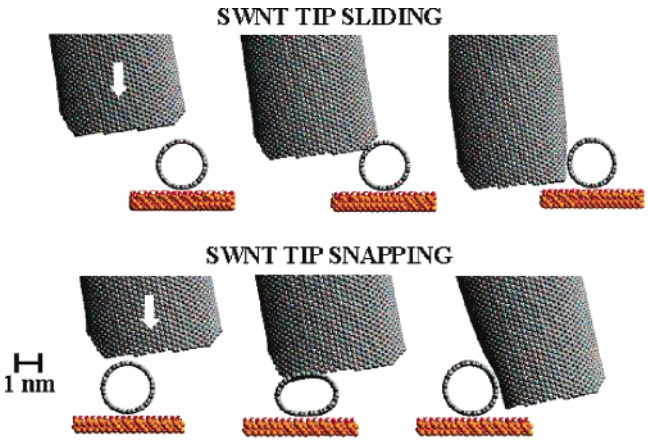

Figure 1. 40,40 SWNT tip imaging a sample 16,16 SWNT in smooth gliding mode (top) and snapping mode (bottom). In the first case, the deformation of the sample is negligible and the tip and sample are able to slide past one another primarily due to tip bending and local deformation. In the second case, the sample nanotube is initially compressed against the substrate, undergoing elastic deformation until the tip snaps off the sample.

The equation of motion for a damped harmonic oscillator is the following:

$$m\frac{d^2z(Z_c,t)}{dt^2} = -kz(Z_c,t) + m\frac{\omega_o}{Q}\frac{dz(Z_c,t)}{dt} + F_{ts}(z_{ts}) + F_o\cos(\omega t) \quad (1)$$

where $z(Z_c,t)$ is the instantaneous tip position with respect to its equilibrium rest position (Z_c), k the harmonic force constant for the displacement of the tip with respect to its equilibrium rest position, m the AFM cantilever's effective mass, $\omega_o = \sqrt{k/m}$ the free resonant frequency, Q the quality factor, z_{ts} the instantaneous tip position with respect to the sample, $F_{ts}(z_{ts})$ the calculated tip−sample interaction force, and $F_o\cos(\omega t)$ the oscillating driving force applied to the cantilever (we used $\omega = \omega_o$ as in our experiments). The oscillation amplitude is obtained directly from the tip trajectory. The phase is obtained from its Fourier transform. Our previous publication describes in detail the software and MD parameters used in the calculations.[13] The references for the MD parameters for Au nanocrystals and Si(111)−CH_3 surfaces are provided in Supporting Information.

In this study we analyze three model cases in detail: (1) 17 nm radius conventional silicon tip tapping on a bare silicon surface; (2) 40,40 SWNT tip tapping on the edge of a 16,16 SWNT sample, such that smooth gliding occurs when the probe descends on the sample as shown at the top of Figure 1; (3) 40,40 SWNT tip tapping on a 16,16 SWNT sample, such that the probe first compresses the sample and then snaps past it as

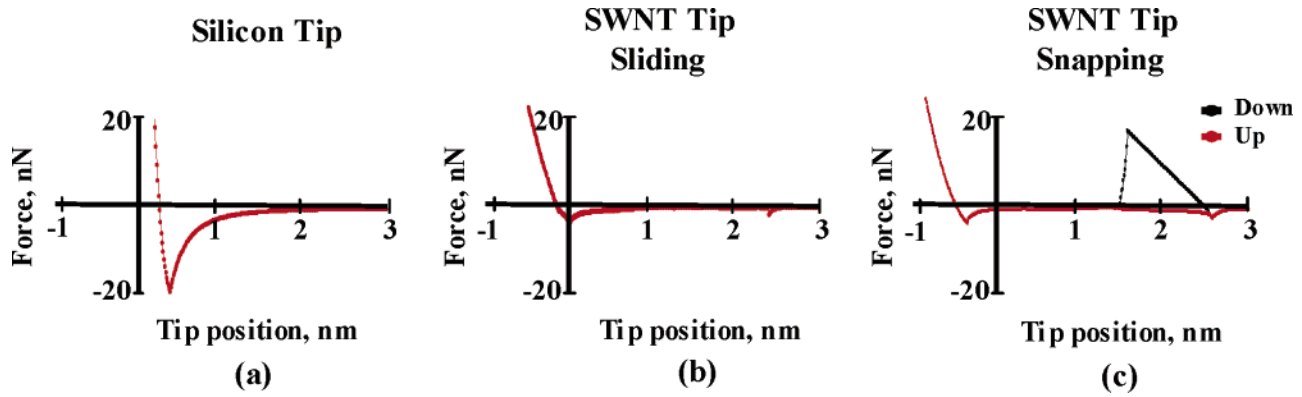

Figure 2. Tip−sample interaction force vs tip position above the surface for a 17-nm-diameter silicon tip imaging a bare silicon surface (a), and for the SWNT tip imaging a prone SWNT in sliding (b) and snapping (c) modes. The tip sample interaction force curve for the SWNT tip imaging a bare silicon surface is similar to curve (b) and is shown in Figure S-2 of the Supporting Information.

shown at the bottom of Figure 1. Our analysis includes more than one variation of case 3, depending on the magnitude of the force required for snapping to occur.

For each of these tip−sample potentials, eq 1 was solved numerically for eight different values of the excitation force amplitude (F_o) corresponding to free oscillation amplitudes (A_o) ranging from 5 to 40 nm in increments of 5 nm, and for cantilever rest positions (Z_c) ranging from 5 to 40 nm above the surface in increments of 0.5 nm. This provided the oscillation amplitude as a function of A_o and Z_c, for a given initial velocity (V_o) and position of the tip. This procedure was repeated for three different values of V_o: 0.0025 nm/s, 0 nm/s, and −0.0025 nm/s. In all cases, the initial tip position was set equal to its equilibrium position, i.e., $z(Z_c,0) = 0$.

The above sets of data for each potential were used to construct the "phase space" representations of the oscillation amplitude solutions as a function of the variables A_o, Z_c, and V_o.

We then constructed amplitude and phase curves (vs Z_c) for tip−sample interaction potentials that exhibited snapping, both with and without the inclusion of adhesive and frictional forces. Adhesive forces were added at the point where the tip first contacts the sample, and at the point where the tip first contacts the substrate surface (after sliding past the sample), acting only during the upward motion of the tip as it was traveling away from the sample. The magnitude of this adhesive force was selected to be within the range given in the work of other authors.[15−17]

The added tip−sample frictional dissipation force was proportional to the negative of the tip velocity, and acted only when tip and sample were in direct physical contact. This friction force was introduced through the use of two different values of the quality factor in the integration of eq 1: the free oscillation quality factor, Q_f, when tip and sample were *not* in contact, and a (significantly lower) contact quality factor, Q_c, when they were in contact and sliding past one another. The effective quality factor, Q, was thus varied between these two values in the integration of eq 1. There is no information available on the magnitude of these tip−sample friction forces during imaging, so we varied the contact quality factor between 0.005 and 0.05 times the free oscillation quality factor until we were able to reproduce the features observed in the experimental results (this is equivalent to assuming that for a given tip velocity, the tip−sample friction forces are between 20 and 200 times greater than the air damping forces experienced by the free oscillating cantilever). Our introduction of a tip−sample dissipation force proportional to the velocity is an approximation similar to that used in describing Newton's law of viscosity for the case of two parallel plates sliding with respect to one another while a Newtonian fluid is being sheared between them.[20] The true nature of the tip−sample interaction forces between SWNT AFM tips and samples depends on atomistic phenomena that are different than those present in a continuum description of a Newtonian fluid, and is expected to exhibit complex, nonmonotonic behavior,[21−24] but the results presented in the next section show that this model is able to reproduce the experimental results qualitatively.

Finally, to generalize our observations to other common geometries, we constructed the tip−sample interaction force curves for a 30,30 SWNT tip imaging a Si(111)−CH_3 surface step edge and a 4.7 nm Au nanoparticle on a Si(100)−OH surface respectively, which we then used to construct the corresponding amplitude and phase curves (vs Z_c) for $A_o = 20$ nm and for $A_o = 10$ nm, respectively, in the absence of tip−sample adhesion and friction forces.

Results

Figure 2 shows the tip−sample interaction force as a function of the tip position above the surface for the three model cases under study, in the absence of tip−sample adhesion and friction forces. Figure 2a is the tip−sample interaction force curve for a conventional 17-nm-radius silicon tip imaging a bare silicon surface. It shows a well-defined long-range attractive region and a short-range repulsive region. Figure 2b, which corresponds to the SWNT smooth gliding mode, shows that the tip−sample interaction force exhibits a local (attractive) minimum just below 2.5 nm as the probe first approaches the sample. It remains slightly negative (attractive) as tip and sample slide past one another, until a second minimum at approximately 0 nm is reached, after which it becomes repulsive and continues to increase monotonically with further downward displacement of the probe. Negative values of the tip position correspond to elastic deformations in the SWNT tip and the sample nanotube upon contact. Note that the tip−sample force remains slightly attractive as the probe and sample glide past one another even though they are both undergoing elastic deformation. MD simulations indicate that this is due to the favorable van der Waals interactions between their graphitic surfaces.

Figure 2c corresponds to the SWNT snapping mode. As the graph shows, the force initially exhibits a local (attractive) minimum when the probe first approaches the sample, and then starts increasing as the sample is compressed (black line). If the probe retracts before reaching a vertical separation of approximately 1.5 nm from the substrate surface (at a force of

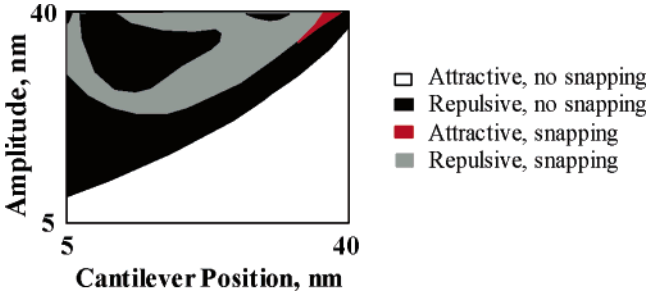

Figure 3. A_o-Z_c phase space representation of the oscillation amplitude solutions for SWNT tip−sample interactions corresponding to Figure 2c for $V_0 = 0$, in the absence of tip−sample adhesion and friction forces. The corresponding phase space representations for $V_0 = -0.0025$ nm/s and $V_0 = 0.0025$ nm/s are qualitatively similar.

approximately 15 nN), it will return to its initial position along the same path it followed to compress the sample. However, if the probe compresses the sample with a force that exceeds 15 nN, it will snap off as shown at the bottom of Figure 1, and the force will immediately decrease to a value close to zero. The probe will continue its downward trajectory until it reaches the substrate surface, where it will initially experience a small attractive force and then an increasingly repulsive force. When the probe retracts it will follow a different trajectory than when it initially approached the sample (red line) because snapping only occurs when the probe is moving downward.

Note that the magnitude of the attractive force at the force curve minimum is several times greater for a conventional tip (Figure 2a) than a SWNT tip (Figures 2b and 2c, and Figure S-2 of the Supporting Information). This is due to the greater number of atoms in the solid silicon tip, which experience strong van der Waals attractions with the substrate surface at short range. Even for the same tip radius, SWNTs have significantly fewer atoms in close proximity to the surface due to their hollow geometries, resulting in much smaller attractive forces.

Numerical integration of eq 1 shows that in the absence of tip−sample adhesion and friction forces, four solutions of the oscillation amplitude are possible for the snapping mode. Two of them− one in the attractive regime and one in the repulsive regime− correspond to the cases when the probe does *not* snap off the sample during the oscillation. If the probe snaps during the oscillation, then two more distinct solutions become available, one of them in the attractive regime and another one in the repulsive regime. Figure 3 shows the A_o-Z_c "phase space" representation of these four solutions for $V_o = 0$, in the absence of tip−sample adhesion and friction forces. The "phase space" representations for the conventional silicon tip and for the SWNT tip in smooth sliding mode, on the other hand, only show two solutions, which correspond to the well-known attractive and repulsive regimes described previously by other authors (Supporting Information).[11,12] The phase space diagram in Figure 3 shows four distinct amplitude solutions. The white region corresponds to an attractive solution where the probe does not snap during the oscillation; the black regions correspond to a repulsive solution where the probe does not snap during the oscillation, the gray regions correspond to a repulsive solution where the probe snaps for every oscillation, and the small red region on the top right-hand side of the diagram corresponds to an attractive solution where the probe snaps for every oscillation. The red region is the smallest of all and corresponds to the cases where the probe has just enough energy to snap off the sample during each oscillation, but is unable to reach the substrate surface. This diagram was constructed using the force curve of Figure 2c.

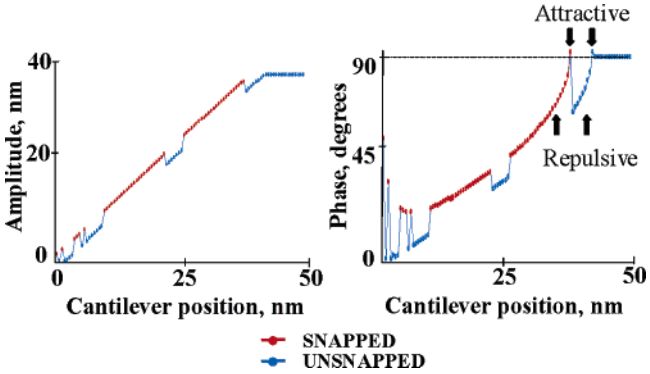

Figure 4. Amplitude and phase vs cantilever position for the SWNT tip−sample interaction in snapping mode, in the absence of tip−sample adhesion and friction forces. The free oscillation amplitude A_0 was 40 nm and the initial tip velocity was set to zero in the simulation. The points where the tip snaps during every oscillation are shown in red and those for which it does not snap are shown in blue. These curves were constructed using force curve (c) of Figure 2.

The AFM tapping mode phase and amplitude curves for the conventional silicon tip and for the SWNT smooth gliding mode as functions of tip−substrate separation distance (Z_c) clearly show the existence of only one attractive and one repulsive solution (Supporting Information).[11,12] The snapping mode amplitude and phase curves, on the other hand, show more diverse behavior. To visualize all the features of this process, we identified the points in the simulated amplitude and phase curves where the probe had snapped off the sample nanotube (Figure 4) with a different color (blue for the cantilever equilibrium positions for which the probe does *not* snap during the oscillation and red for the points for which it *does* snap during the oscillation). These curves correspond to a free oscillation amplitude (A_o) of 40 nm and an initial tip velocity (V_o) of zero. We note that the amplitude curve does not directly reveal transitions involving the long-range attractive (white areas in Figure 3), long-range repulsive (black areas in Figure 3), and short-range attractive solutions (red areas in Figure 3) to eq 1. The only distinct jumps in the amplitude curve are those between the two repulsive solutions, one of which corresponds to the probe snapping every oscillation period of the tip (gray areas in Figure 3), and the other one to oscillations where snapping does not occur (black areas in Figure 3). The phase curve, however, *does* show all four solutions clearly, as well as the points where the system jumps between them. Most of the jumps correspond to jumps between the repulsive solutions (the phase is below 90° before and after the jump). This is consistent with the phase space diagram of Figure 3, which shows large borders between adjacent regions corresponding to repulsive solutions.

In the Supporting Information we provide phase and amplitude curves for the case when a 25 nN tip−sample adhesion force is added to force curve (c) of Figure 2. In this case, both attractive solutions and one repulsive solution are clearly discernible from the amplitude and the phase curves. The long-range repulsive solution does not occur due to the large adhesion (attractive) force, which dominates the interactions when the probe does not snap. These results suggest that adhesion forces can magnify the difference between the different solutions.

Figures 5a, 5b, and 5c contain experimental results for a SWNT tip imaging a SWNT sample on a silicon oxide substrate, for low, intermediate, and high values of A_o, respectively. In all three cases the SWNT tip was tapping directly on the crown of the sample SWNT. The phase curve of Figure 5a exhibits a predominantly attractive regime, in *disagreement* with the theoretical simulation of Figure 4, which does not consider tip−

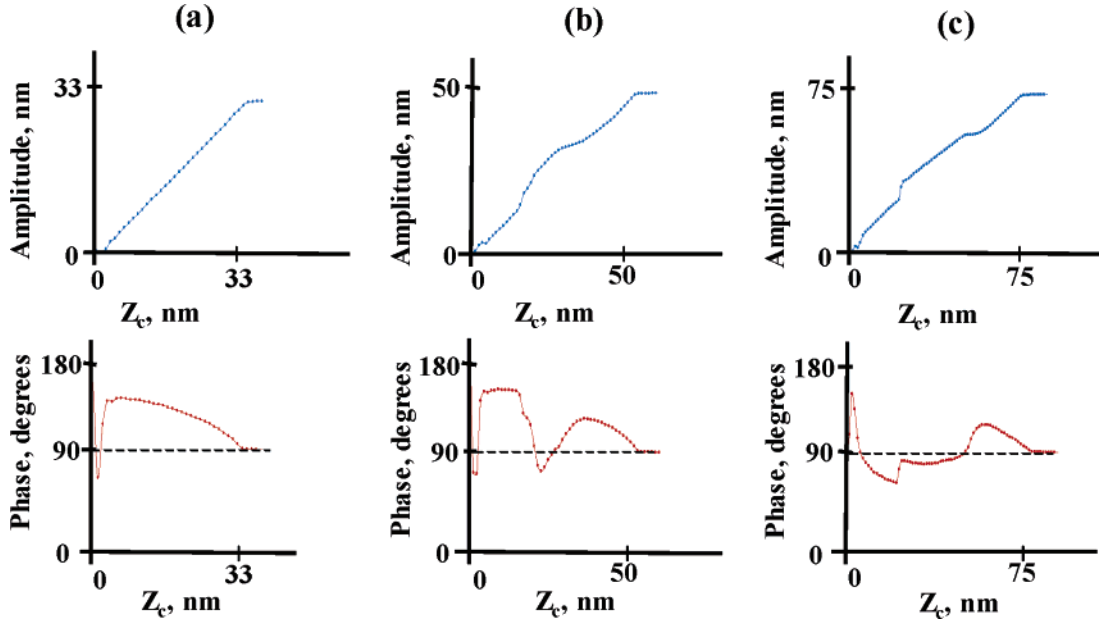

Figure 5. Experimental amplitude and phase vs Z_c for a SWNT tip tapping directly on top of a sample SWNT on a silicon oxide substrate, for different values of the free oscillation amplitude (A_0): (a) $A_0 = 33$ nm, (b) $A_0 = 50$ nm, (c) $A_0 = 75$ nm.

sample adhesion and friction forces. Figures 5b and 5c show smooth variations of the phase and amplitude as the cantilever approaches the sample, including phase transitions between attractive and repulsive regimes *without* a discontinuity. Figure 5c shows that it is also possible to have smooth variations between the attractive and repulsive regimes *and* discontinuities on the same curve. The discontinuity of this curve, where the phase jumps from a value below 90° to a lower value, is similar to the jumps observed in Figure 4, indicating a transition between a regime where the probe snaps during each oscillation (henceforth referred to as a "snapped oscillation") to a regime where the probe does not snap during the oscillation (henceforth referred to as an "unsnapped oscillation"), as the cantilever equilibrium position, Z_c, is lowered. The relative magnitude of the phase between the snapped and unsnapped oscillations is consistent with Figure 4, which shows that the phase is higher for snapped oscillations than for unsnapped oscillations. This is also consistent with the magnitude of the oscillation amplitude before and after the jump, which indicates that the oscillation amplitude is greater when snapping occurs. The amplitude curve shows two transitions, one from an unsnapped oscillation to a snapped oscillation, and one from a snapped oscillation back to an unsnapped oscillation. Although the first transition is not as evident in the phase curve, this curve has an inflection point, which indicates a change in the nature of the tip−sample interaction.

We also observed curves with similar behavior to that of a conventional silicon tip, although the range of Z_c corresponding to the attractive region was generally much larger. In general, the experimental measurements show significantly greater attractive regions than those calculated based on van der Waals interactions alone, suggesting the presence of other attractive interactions, such as capillary or electrostatic forces.

Figure 6 shows three theoretical simulations using different snapping potentials where we have explicitly included tip−sample adhesion and frictional forces, as described above in the theoretical methods section. All three simulated phase curves in Figure 6 are in close qualitative agreement with their experimental counterparts in Figure 5, although the transitions in the experimental amplitude curves in Figure 5 are more pronounced than in the corresponding simulations (see discussion below Figure 6). The curves in Figure 6a, which were constructed using the force curve of Figure 2c, indicate that the tip did not snap during the oscillation until the separation distance to the surface was nearly zero (indicated by the sharp minimum in the phase curve when Z_c approaches zero) and that the predominantly attractive region is a consequence of the large tip−sample adhesion and frictional components that were included in the tip−sample interaction.

Curves 5b and 6b correspond to cases where the force barrier is too high or the excitation force is too low for snapping to occur, and both attractive regions are a consequence of the adhesion force at the point of tip−sample contact, magnified by the friction force. As Z_c decreases in curve 6b, the phase initially increases due to the adhesion force. It gradually shows a decrease, becoming smaller than 90° as the probe begins to experience a repulsive force, and then increases when the adhesion force once again becomes dominant at even lower values of Z_c. The amplitude curve shows a smooth gradual increase and decrease, indicating the transitions from attractive to repulsive and from repulsive back to attractive regimes.

The simulations show that as the tip−sample friction forces increase (i.e., as Q_c is lowered), the transitions between attractive and repulsive regimes become smoother because the larger friction forces allow the probe to more gradually approach and move away from the sample during every oscillation, which causes the average tip−sample interaction force to vary smoothly from positive to negative and vice-versa.

The phase curve of Figure 6c is similar to that of Figure 5c, except that it shows both snapping transitions clearly. This simulation was performed using different values of the friction and adhesion forces for snapped and unsnapped oscillations. The maximum of the adhesion force was set to 20 nN for unsnapped oscillations and to 5 nN for snapped oscillations (this is reasonable since MD simulations show that the tip−sample contact area is significantly smaller after the tip snaps). The contact quality factor for snapped oscillations was set to 90% of the value for unsnapped oscillations.

The probe was unable to reach the surface in any of the simulations corresponding to Figure 6, and thus the tip−substrate surface adhesion force did not play a role. The simulated amplitude curves in Figure 6 do not show the sharp transitions

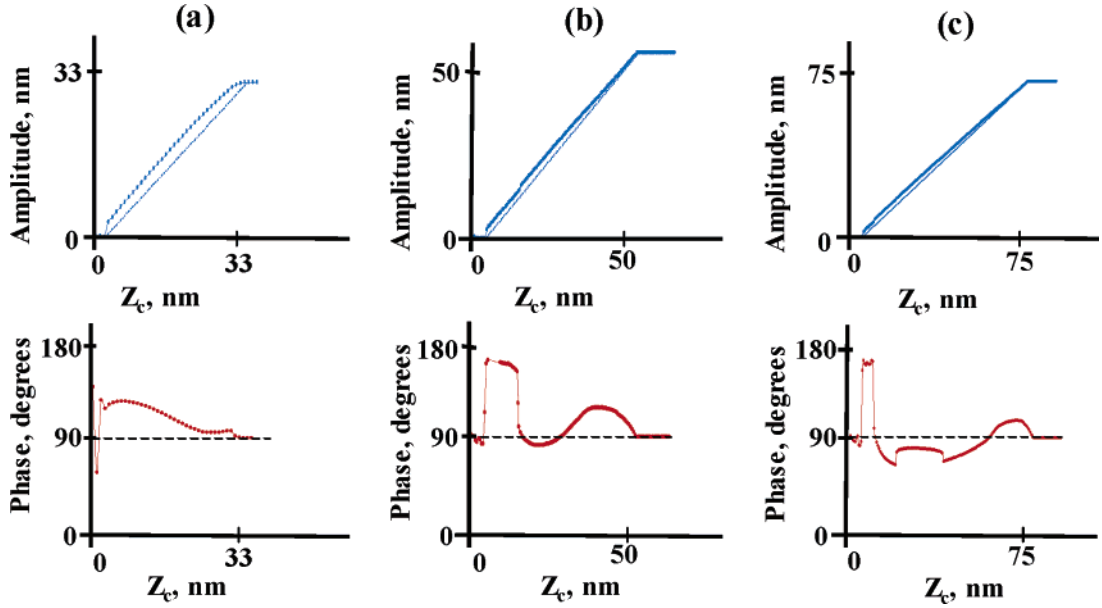

Figure 6. Simulated amplitude and phase vs Z_c for snapping potentials with the inclusion of adhesion and friction forces for different values of the free oscillation amplitude (A_0): (a) $A_0 = 33$ nm, (b) $A_0 = 50$ nm, (c) $A_0 = 75$ nm. We have included straight dotted lines for easier visualization of the curvature of the amplitude curves. The adhesion and friction force parameters are provided in the Supporting Information.

observed experimentally in Figure 5, although they do show smooth changes in slope that indicate gradual transitions from one regime to another. Within our model, these transitions in the amplitude curves are more pronounced for small values of the friction force (i.e., for large values of Q_c, such as in Figure 4) but gradually disappear as the friction force increases (i.e., as Q_c is lowered), which reduces the distance that the probe is able to travel freely after snapping off the sample. The simulations corresponding to Figure 6 were performed using relatively low values of Q_c (increased friction) in order to match the experimental phase curves as closely as possible, which we found to be more useful in our discussion of tapping-mode AFM multistability.

In the Supporting Information we provide the tip−sample energy and force curves, and the amplitude and phase curves for the SWNT tips imaging a Si(111)−CH_3 surface step edge and a Au nanoparticle. These curves exhibit features similar to those of Figure 2c and Figure 4, respectively, indicating that snapping can occur, and hence multiple solutions to the oscillation amplitude are also possible for these types of samples.

Discussion

Silicon Tips vs SWNT Tips. It is commonly accepted that the oscillation amplitude of an AFM cantilever, which can be closely modeled using the damped harmonic oscillator approximation (eq 1), has only two solutions that are physically meaningful. However this knowledge is based on the assumption that the tip−sample interaction potential has the general shape of a Morse or Lennard-Jones curve, where the potential is monotonically attractive at long ranges and monotonically repulsive at short ranges. Two of the model cases analyzed in this study, the SWNT smooth gliding mode and the conventional silicon tip, correspond approximately to potentials of this type, and when integrated into eq 1 do yield two solutions for the amplitude in the absence of tip−sample adhesion and friction forces.

Although the results for these two cases are qualitatively similar, there are some differences that are worth discussing. First, we note that the damping of the oscillation amplitude of the SWNT tip, due to interactions with the sample, is less than that of a conventional silicon tip for a given value of Z_c and F_o, indicating greater penetration into the sample and surface as well as greater local elastic deformation of the nanotube, as confirmed through molecular simulations. This is an important consideration regarding the use of SWNTs for topographical imaging, because it indicates that while SWNT tips are able to image high aspect features such as trenches and crevices in finer detail than silicon tips, as one would expect from their dimensions, they may not always provide an accurate representation of the sample due to local deformation, especially in highly repulsive regimes where the tip−sample interaction forces can be significant.

Another important difference between SWNT tips and conventional tips is that changes in both the attractive and repulsive forces are steeper functions of tip position for silicon tips than for SWNT tips (as shown in Figure 2). Silicon tips experience greater van der Waals attractive forces when close to the surface due to the larger number of atoms in the tip. The range of cantilever rest positions resulting in a long-range attractive solution should be significantly smaller for a nanotube probe compared to a conventional silicon tip because the attractive forces are smaller and operate over a shorter range. This means that for clean SWNTs, for which dispersion forces are the main interactions, most of the imaging is expected to take place in the repulsive regime.[5] Our calculated tip−sample van der Waals forces are in agreement with the tight-binding calculations of Tagami et al. on clean tips and surfaces, which show maximum values of 1−1.5 nN for a fullerene tip on a silicon surface.[25,26] On the other hand, our calculated forces are significantly lower than those obtained from treating the SWNT tip as a sphere using the Hamaker equation; however, we feel this treatment is not adequate for a SWNT tip because such a tip is not a solid continuum sphere,[19] and also because such an approximation neglects the local structural changes, as well as the bending and sliding phenomena that can take place when SWNT tips are used. Although the use of the Hamaker equation of a sphere may in some cases give qualitatively satisfying results, these should be interpreted with caution, because this

agreement may be a mathematical artifact and not necessarily an accurate description of the dynamics of the system.

Snapping. Understanding the snapping phenomenon of SWNT tips is fundamental to the development of SWNT AFM techniques. We have previously shown that snapping and sliding effects have direct influence on the probe resolution and measured sample width.[13] The results presented here show that snapping can also give rise to multiple solutions of the oscillating amplitude, including a continuum of solutions when large adhesion and friction forces are present.

A quick glance at the amplitude curve in Figure 4 might suggest that it describes an imaging process with the usual bistability. [11,12] However, a closer analysis of the snapping potential (Figure 2c) and the phase curve (Figure 4) reveals that the long-range portion of the potential gives rise to two imaging solutions when the excitation force is small (too small to overcome the snapping barrier) or the probe is sufficiently far away from the sample. Two more solutions appear when the probe is able to snap off the sample, due to a second overall attractive regime and a second overall repulsive regime. The phase space diagram of Figure 3 shows that the repulsive solutions dominate the attractive solutions in the region where the probe and the sample are in contact ($Z_c < A_o$) in the absence of tip−sample adhesion and friction forces. The relative dominance of the repulsive solutions is a consequence of the particular tip−sample interaction potentials analyzed here and can be different for different tips and samples, but the existence of multiple solutions should be common to all tip−sample interaction potentials that exhibit snapping. This is confirmed by our simulations of SWNT tips imaging Si(111)−CH_3 surface step edges and Au nanocrystals (Supporting Information).

Importance of Adhesion and Friction. The experimental results for imaging with SWNT tips in Figure 5 show that the process takes place primarily in an attractive regime, in disagreement with the theoretical simulations of clean surfaces and samples. This indicates that either there is a significantly stronger attraction or adhesion of the SWNT tips to the surface than that corresponding to the van der Waals interactions alone, or that there are other important effects that have not been included in the equation of motion, which magnify the effect of the small van der Waals attractive forces.

Jang et al. and Stifter et al.[15−17] have shown that the adhesive force of the AFM tip to the surface mediated by a water meniscus can be significant and in some cases dominant over the van der Waals forces (on the order of tens of nN). Lee et al. measured the adhesive force of a 10 nm multiwall nanotube tip to the surface and also showed that it is on the order of tens of nN.[18] Although clean SWNT tips are hydrophobic, it is possible that the ends are open and oxidized to form hydrophilic functional groups (such as carboxylate groups), especially when the fabrication procedures include severe treatments such as shortening through electric discharges between the tip and surface.[6] In this case it is likely that capillary forces play an important role in the imaging process.

As described in the methods section, we modeled the adhesion forces using values up to 25 nN with various decaying functional dependences on the tip position (see Supporting Information). Additionally, we find that the dissipation term in the cantilever equation of motion is not sufficient to account for the tip−sample friction forces since it only includes the friction of air acting on the oscillating cantilever. These friction forces can be modeled with a dissipation term that is proportional to tip velocity in a manner similar to Newton's law of viscosity,[20] with adjustment of an effective quality factor to achieve the correct order of magnitude agreement with experimental data. There is no easy way to determine this magnitude and very little is known about these friction forces, but we can imagine that if frictional forces significantly affect the cantilever oscillation, they should be able to dissipate similar amounts of energy as the air damping forces, and since they act over much smaller distances, their effective quality factor should be much smaller than the free air quality factor (the coefficient of the dissipation term is inversely proportional to the quality factor in eq 1). We used contact quality factor values between 0.005 and 0.05 times the free oscillation value, which allowed us to obtain results similar to those obtained experimentally (compare Figures 5 and 6).

In our previous report[13] we presented a simulation of the cross-sectional scan of a prone SWNT, which shows "negative" height readings in the regions where the probe snapped or slid past the sample, in disagreement with the experimental result. These negative readings in the simulated scan were due to the probe bending around the sample before reaching the surface, which increased the distance the probe had to descend in order to reach the surface. The results presented here show that friction forces can prevent the tip from reaching the surface, thus reconciling our simulations with our experimental observations.

The experimental results of Figure 5 and the theoretical simulations of Figure 6 show that dissipation effects can also give rise to a continuum of amplitude solutions, in addition to (or instead of) the usual discontinuous jumps between attractive and repulsive regimes. We can visualize this continuum of amplitude solutions as a collection of amplitude curves of the same slope, each corresponding to a different amplitude solution (as in the case of bistability, but with a greater number of solutions), which allow the amplitude to vary with arbitrary slope between smaller and larger values. Our results show that as the tip−sample friction increases, the separation between the different regimes becomes smaller, indicating that the number of possible solutions increases and the separation between them decreases. In the limit of large friction, the number of solutions should be infinite.

Lee and co-workers[18] reported that their experimental measurements with a multiwall carbon nanotube tip did not show evidence of two coexisting regimes as is the case with regular tips, and although the dimensions of their tip and the geometry of their sample are significantly different than ours, it is possible that their results can also be explained through the introduction of dissipation and adhesion effects that are present when nanotube tips are used. We point out that in this study we have assumed that all sliding phenomena whose friction forces significantly affect the tip oscillation occur between the tip and the sample, but it is also possible that slipping occurs at the attachment between the SWNT tip and the supporting silicon tip, which are kept in place primarily through van der Waals forces (significantly weaker than those due to covalent bonds).

Practical Implications of Multistability. It is well known that imaging parameters which lead to bistability[11,12] must be avoided in order to obtain good AFM images, so it is logical to expect the SWNT multistability phenomena described here to also affect image quality significantly. We have shown that these effects are different from bistability in that they include a combination of more than one single interaction potential (between the tip, the sample and the substrate) with dissipative forces (adhesion and friction), and that they can be explained in terms of individual components related to each type of interaction. Below we discuss the practical implications of each effect separately.

The interaction of the SWNT probe with the substrate is responsible for the existence of one attractive and one repulsive amplitude solution, which occurs as a result of the coexistence of an attractive and a repulsive regime in the same tip−sample interaction potential. This has been extensively discussed by numerous authors[11,12] and our work reveals no additional knowledge.

Snapping and sliding phenomena, and the existence of additional attractive and repulsive amplitude solutions, as depicted in Figure 4, result from the interactions between the probe and the sample. These effects are not desired because they can distort the dimensions of the image[13] but can be minimized by selecting the appropriate probe geometry, as discussed extensively in ref 6. In general, snapping and sliding are most likely to occur for probes that are highly tilted ($> 30°$ with respect to the vertical axis), too long (> 55 nm for SWNT probes 5.5 nm in diameter), or with too high an aspect ratio (> 10). Irregular probe geometries on the imaging end can also be a contributing factor to these artifacts. Probes of lower aspect ratio, which are less likely to bend, can be advantageous, but using them requires caution, since extremely short probes (<20 nm long) can also cause shadowing due to the long-range interaction forces between the sample and the supporting silicon tip.[6] Local tip deformation can be reduced by using SWNTs of smaller diameters, but this requires using shorter probes due to the softer bending modes of thinner SWNTs. Finally, snapping can be minimized by imaging at lower oscillation amplitudes and higher amplitude setpoints, corresponding to less repulsive regimes, which prevent the tip−sample interaction force from reaching the snapping point (see Figure 2c).

The third and last aspect of multistability concerns the gradual transitions between attractive and repulsive regimes, described in Figures 5 and 6. The high quality images[6] obtained with the probe used to obtain our experimental results suggest that this effect does not significantly affect image quality, as long as the sharp transitions between attractive and repulsive imaging regimes are avoided.

Thus the practical considerations for avoiding the deterioration of image quality due to multistability are the same as those used for selecting high quality SWNT probes[6] and avoiding bistability,[11,12] in addition to evading the highly repulsive regimes that favor the occurrence of snapping.

Conclusions

We have highlighted fundamental differences in the tip−sample interactions between conventional silicon tips and SWNT tips used in tapping-mode AFM imaging and have explained the effects of explicit tip−sample adhesion and friction forces. We have also shown that these interactions can be modeled through the individual inclusion of each effect into the equation of motion of a damped harmonic oscillator, thus providing insightful analytical connections between theory and experiment.

There are many sources of uncertainty that could explain the quantitative differences between our experimental and theoretical results, such as the knowledge of the exact relative position of tip and sample in the experiment, the exact tip and sample geometry, the nonlinearity of the tip position with respect to the supporting silicon tip position when the probe deforms, the presence of moisture and impurities on the surface, the exact behavior of adhesion forces, the true nature of the tip−sample friction forces, etc., but, nevertheless, the agreement between theory and experiment is remarkable with this simple model. More detailed theoretical and experimental research is required with more sophisticated assumptions of the tip−sample interaction, which we plan to address in greater detail in a future publication.

Acknowledgment. S.D.S. and W.A.G. were supported by the Microelectronics Advanced Research Corporation (MARCO) and its Focus Center on Function Engineered NanoArchitectonics (FENA). M.J.E. and C.P.C. were supported by Arrowhead Research.

Supporting Information Available: TEM image of SWNT probe used in calculations, experimental procedure for imaging on crown of sample SWNT, additional tip−sample force curve, phase space representations, and phase and amplitude curves, adhesion and friction force parameters, simulation results for other sample geometries, and additional molecular dynamics simulation parameters. This material is available free of charge via the Internet at http://pubs.acs.org.

References and Notes

(1) Bushnan, B.; Kasai, T.; Nguyen, C. V.; Meyyappan, M. *Microsys. Technol.* **2004**, *10*, 633.
(2) Uchihashi, T.; Choi, N.; Tanigawa, M.; Ashino, M.; Sugawara, Y.; Nishijima, H.; Akita, S.; Nakayama, Y.; Tukumoto, H.; Yokoyama, K.; Morita S.; Ishikawa, M. *Jpn. J. Appl. Phys.* **2002**, *39*, 887.
(3) Umemura, K.; Komatsu, H.; Uchihashi, T.; Choi, N.; Ikawa, S.; Nishinaka, T.; Shibata, T.; Nakayama, Y.; Katsura, S.; Mizuno, A.; Tokumoto, H.; Ishikawa M.; Kuroda, R. *Biochem. Biophys. Res. Commun.* **2001**, *281*, 390.
(4) Bunch, J. S.; Rhodin, T. N.; McEuen, P. L. *Nanotechnology* **2004**, *15*, S76.
(5) Chen, L.; Cheung, C.-L.; P. Ashby, P.; Lieber, C. M. *Nano Lett.* **2004**, *4*, 1725.
(6) Wade, L. A.; Shapiro, I. R.; Ma, Z.; Quake, S. R.; Collier, C. P. *Nano Lett.* **2004**, *4*, 725.
(7) Hafner, J. H.; Cheung, C. L.; Woolley, A. T.; Lieber, C. M. *Prog. Biophys. Mol. Biol.* **2001**, *77*, 73.
(8) Guo, L.; Liang, J.; Dong, S.; Xu, Z.; Zhao, Q. *Appl. Surf. Sci.* **2004**, *228*, 53.
(9) San Paulo, A.; García, R. *Biophys. J.* **2000**, *78*, 1599.
(10) Thomson, N. H. *J. Microscopy* **2005**, *217*, 193.
(11) García, R.; Perez, R. *Surf. Sci. Rep.* **2002**, *47*, 197.
(12) García, R.; San Paulo, A. *Phys. Rev. B* **1999**, *60*, 4961.
(13) Shapiro, I. R.; Solares, S. D.; Esplandiu, M. J.; Wade, L. A.; Goddard, W. A.; Collier, C. P. *J. Phys. Chem. B* **2004**, *108*, 13613.
(14) Hafner, J. H.; Cheung, C.-L.; Oosterkamp, T. H.; Lieber, C. M. *J. Phys. Chem. B* **2001**, *105*, 743.
(15) Jang, J.; Schatz, G.; Ratner, M. *J. Chem. Phys.* **2004**, *120*, 1157.
(16) Jang, J.; Schatz, G.; Ratner, M. *Phys. Rev. Lett.* **2003**, *90*, 156104−1.
(17) Stifter, T.; Marti, O.; Bhushan, B. *Phys. Rev. B* **2000**, *62*, 13667.
(18) Lee, S. I.; Howell, S. W.; Raman, A.; Reifenberger, R.; Nguyen, C. V.; Meyyappan, M. *Nanotechnology* **2004**, *15*, 416.
(19) Snow, E. S.; Campbell, P. M.; Novak, J. P. *J. Vac. Sci. Technol. B* **2002**, *20*, 822.
(20) McQuarrie, D. A. *Statistical Mechanics*; University Science Books: Sausalito, CA, 2000, 360−362.
(21) Dickrell, P. L.; Sinnott, S. B.; Hahn, D. W.; Raravikar, N. R.; Schadler, L. S.; Ajayan, P. M.; Sawyer, W. G. *Tribol. Lett.* **2005**, *18*, 59.
(22) Reimann, P.; Evstigneev, M. *New. J. Phys.* **2005**, *7*, 25.
(23) Zhang, L.; Leng, Y.; Jiang, S. *Langmuir* **2003**, *19*, 9742.
(24) Tsukruk, V. V.; Everson, M. P.; Lander, L. M.; Brittain, W. J. *Langmuir* **1996**, *12*, 3905.
(25) Tagami, K.; Tsukada, M. *Surf. Sci.* **2001**, *493*, 56.
(26) Tagami, K.; Sasaki, N.; Tsukada, M. *Appl. Surf. Sci.* **2001**, *172*, 301.